Materials Science and Engineering A 398 (2005) 77–81

www.elsevier.com/locate/msea

# Three-point bending of electrospun $TiO_2$ nanofibers

Sung-Hwan Lee [a], Cagri Tekmen [b], Wolfgang M. Sigmund [a,*]

[a] *Department of Materials Science and Engineering, University of Florida, PO Box 116400, 225 Rhines Hall, Gainesville, FL 32611, USA*
[b] *Department of Metallurgical and Materials Engineering, Dokuz Eylul University, Bornova, Izmir 35100, Turkey*

Received 8 October 2004; received in revised form 28 February 2005; accepted 11 March 2005

**Abstract**

$TiO_2$ (anatase) and $TiO_2$/PVP nanocomposite nanofibers with average diameters of 53 and 109 nm, respectively, were synthesized via sol–gel chemistry in combination with an electrospinning process. This produced continuous nanofibers that were characterized by scanning electron microscopy (SEM), X-ray diffraction (XRD) and transmission electron microscopy (TEM). $TiO_2$ nanofibers were obtained through thermal oxidation of $TiO_2$/PVP in air and the weight loss was determined by thermal gravimetric analysis (TGA). Mechanical properties were studied with a nanoscale three-point bending test. Elastic properties of single nanofibers are reported as measured by atomic force microscopy (AFM) three-point bending on a mesoporous membrane as support. The mean of elastic moduli for $TiO_2$ and $TiO_2$/PVP nanofibers were found to be 75.6 and 0.9 GPa, respectively.


*Keywords:* Nanofiber; Young's modulus; Titania; Electrospinning; AFM; Three-point bending test

## 1. Introduction

Nanoscale materials, such as nanowires, nanorods, nanowhiskers, and nanofibers have recently attracted attention due to their exceptional properties and novel potential applications. Furthermore, $TiO_2$ as a semiconductor material with special electronic properties allows for applications in environmental remediation and protection, photocatalysis, dye-sensitized solar cells, gas sensors, and batteries [1–10]. Various preparation methods for $TiO_2$ whiskers, nanorods, and nanotubes, including sol–gel, dip-coating, and electrochemical methods have been reported [11–14]. Recently, a new approach has been developed to obtain $TiO_2$ nanofibers by electrospinning of precursor solutions [15–17]. Furthermore, it was recently reported that nanocrystalline $TiO_2$ can be ductile at low temperature (plastic bending at 180 °C, hardness reduction of ∼800 HV at 20 °C) because of the diffusional flow of atoms along the crystalline interfaces [18].

Electrospinning has been widely studied because of its efficiency and simplicity for the production of fibrous materials on micro- or nanosize scale [19–22]. It has been demonstrated that metal oxide nanofibers can be readily synthesized with a combination of sol–gel and electrospinning methods [15–17,21–24]. Since electrospun nanofibers are based on nanocrystal networks they should follow the above mentioned ductility trend, i.e., have mechanical and electronic properties different from micron-size grains and micron-size fibers. In an earlier report, we demonstrated electrospun $TiO_2$–Ag composite nanofibers [17]. In this paper we focus on pure and composite nanofibers and look into their nanomechanical behavior for application purposes, such as photocatalytic filtration media. Since the characterization of such nanofiber materials is still a challenge, we adapt a method that has recently been published for polymer nanofibers and extend it to polymer–ceramic composites and ceramic nanofibers [25–28].

## 2. Experimental—Sample preparation

In the electrospinning process, a viscous sol is prepared and injected at a constant rate through a conductive capillary where high voltage (up to 3 kV/cm) is applied. Charge

* Corresponding author. Tel.: +1 352 846 3343; fax: +1 352 392 6359.
*E-mail address:* wsigm@mse.ufl.edu (W.M. Sigmund).

0921-5093/$ – see front matter © 2005 Elsevier B.V. All rights reserved.
doi:10.1016/j.msea.2005.03.014

is induced on the sol surface by an electric field. Mutual charge repulsion causes a force directly opposite to the surface tension. When the surface charge overcomes the surface tension, a Taylor cone will develop and the electrically charged sol–jet is ejected from the tip of the Taylor cone [19]. In this study, Ti(IV)-isopropoxide (Ti(O*i*Pr)$_4$, Aldrich) was used to form anatase. 1.5 mL of Ti(O*i*Pr)$_4$, and 3 mL of acetic acid were added to 10 mL of ethanol containing poly(vinyl pyrrolidone) (PVP, Aldrich, $M_w$ 1,300,000). The sol was stirred in a capped bottle for 30 min. The prepared sol was ejected from the conductive stainless steel capillary (22 gauge) at a flow rate of 0.5 cc/h with an electric field of 2 kV/cm, where the voltage and distance were set to 10 kV, and 5 cm, respectively. Commercial anodized alumina ultrafiltration membranes (Whatman Anodisc, pore size 200 nm) were used to collect a PVP–$TiO_2$ composite nanofiber mat. The collected samples were dried in air for one day to reduce the impact of stress in the fiber due to synereses. In order to prepare $TiO_2$ nanofibers, the sample was calcined in air at 500 °C for 2 h in order to remove PVP and to crystallize $TiO_2$.

The indentation of the AFM probe into a sample surface offered a direct approach to determine elastic properties by measuring the sensor response to the Z-piezo displacement. The AFM (dimension 3100, Digital Instruments) was used to apply a load at the middle of the suspended nanofiber with a silicon nitride cantilever. AFM measurements were performed in ambient conditions and the upper force limit was set to 6 nN. This maximum force was not sufficient to cause an indent on portions of nanofibers. Thus, it was assumed that the load was not used for the permanent deformation of the sample.

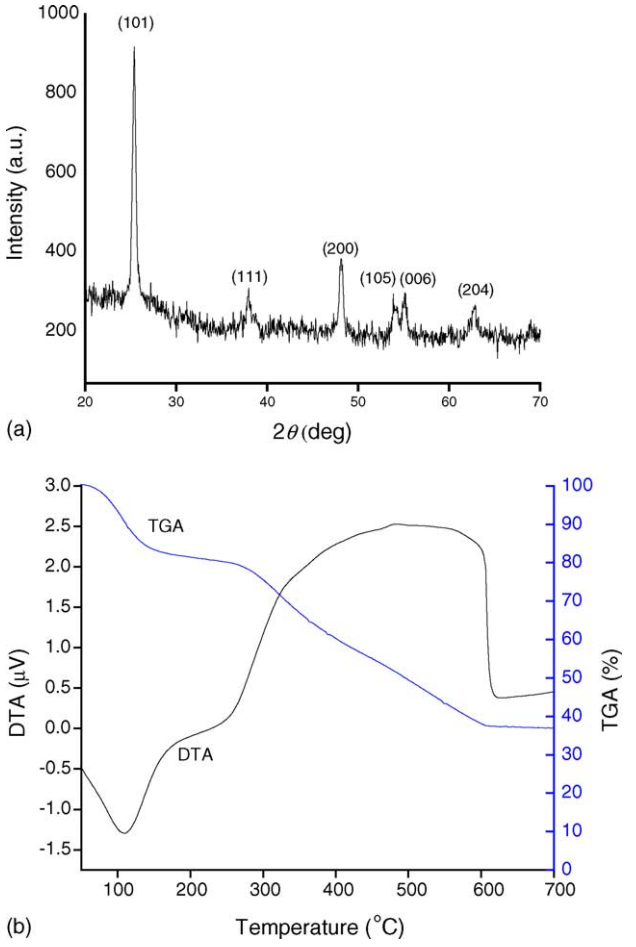


Fig. 1. (a) XRD pattern of heat-treated $TiO_2$ (anatase phase) nanofibers after calcination and (b) TGA/DTA curves (10 °C/min ramp rate).

## 3. Results and discussion

XRD pattern confirmed that $TiO_2$ nanofibers had 100% anatase phase (Fig. 1a) after calcination at 500 °C for 2 h. $TiO_2$ and $TiO_2$/PVP nanofibers had mean diameters of 52.4 and 109.4 nm, respectively. The diameter reduction in $TiO_2$ nanofibers mainly occurred by PVP removal during calcination in air (thermal oxidation). Weight loss was measured with TGA/DTA (ramp rate 10 °C/min) and the result showed the weight loss was in the range of more than 60% (Fig. 1b). The morphology of each sample was studied with SEM before and after the calcinations (Fig. 2a and b) and the mean diameters were obtained. The electrospun nanofibers were collected on $Al_2O_3$ membrane for AFM three-point bending tests to determine Young's modulus (Fig. 2c).

Thermally or electric field induced vibration with transmission electron microscopy (TEM) could be used to measure physical and mechanical properties of individual carbon nanotubes [29,30]. However, its application was limited because it requires a special experimental setup in a vacuum chamber for the in situ TEM analysis. On the other hand, elastic properties of nanofibers can be readily measured with a three-point bend test by preparing a single nanofiber suspended over an empty space and applying a small deflection at the middle of the nanofiber along its suspended length with an AFM cantilever in contact mode. A schematic diagram of the elasticity measurements and AFM scanned cross-sectional profiles of the nanofiber and $Al_2O_3$ membrane pore are given in Fig. 3b. The pore diameter ($L$) and fiber diameter ($D$) obtained by AFM scanning data are presented in Table 1. This method, which has been used to determine the mechanical properties of polymeric nanofibers and carbon nanotubes, enabled the direct determination of the applied force as a function of displacement [25–28].

The applied load ($F$) was measured by collecting a force curve, which is a plot of cantilever deflection as a function of sample position along the $Z$-axis. The load ($F$) applied by the cantilever to the tip surface contact was calculated based on deflection using Hooke's law, where $k$ is the cantilever spring constant. It assumes a simple relationship between the load ($F$), and the deflection given by Eq. (1), where $k$ is the spring constant of the cantilever.

$$F = -k(d - d_o) \quad (1)$$

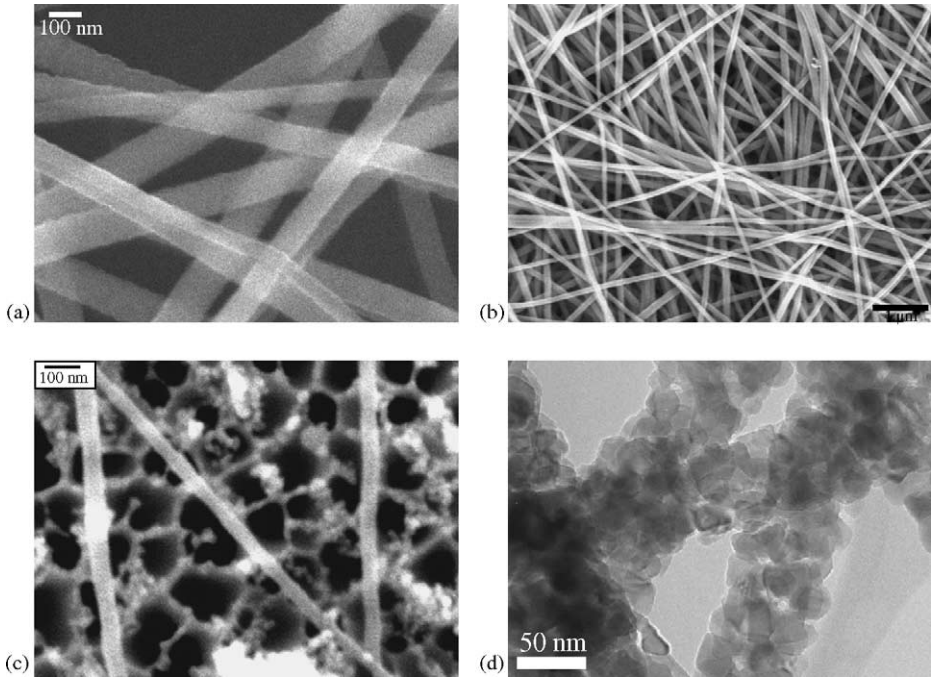


Fig. 2. SEM images of (a) $TiO_2$/PVP nanofibers, (b) $TiO_2$ nanofibers, (c) $TiO_2$ nanofibers suspended over pores of $Al_2O_3$ membrane, and (d) TEM image of $TiO_2$ nanofibers.

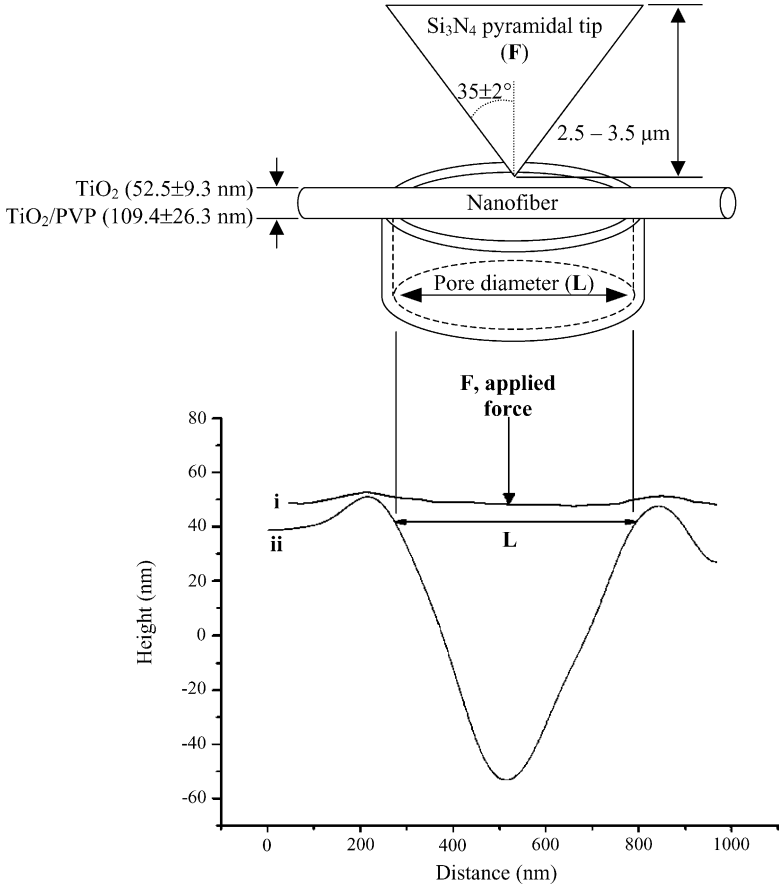


Fig. 3. (a) Schematic diagram of three-point bending test and (b) actual AFM scanning data on fiber (i) and pore (ii).

Table 1
Diameters ($D$), suspended lengths ($L$), and Young's moduli ($E$) for nanofibers

| Sample | $D$ (nm) | $L$ (nm) | $E$ (GPa) |
|---|---|---|---|
| | 118 | 400 | 0.47 |
| | 139 | 350 | 0.40 |
| | 68 | 240 | 2.33 |
| $TiO_2$/PVP | 84 | 374 | 1.00 |
| nanofiber | 77 | 285 | 1.20 |
| (un- | 133 | 366 | 0.33 |
| fired) | 148 | 396 | 0.47 |
| | 107 | 320 | 0.73 |
| | 94 | 285 | 1.47 |
| | 126 | 336 | 0.40 |
| Mean $\pm \sigma$ | $109.4 \pm 26.3$ | $335.2 \pm 49.9$ | $0.9 \pm 0.6$ |
| | 53 | 323 | 64.6 |
| | 50 | 349 | 64.0 |
| | 46 | 252 | 124.6 |
| | 42 | 332 | 72 |
| $TiO_2$ | 51 | 280 | 61.3 |
| nanofiber | 72 | 286 | 52.0 |
| (fired) | 59 | 342 | 70.0 |
| | 61 | 371 | 61.3 |
| | 53 | 294 | 70 |
| | 38 | 276 | 116.6 |
| Mean $\pm \sigma$ | $52.5 \pm 9.3$ | $310.5 \pm 36.3$ | $75.6 \pm 23.2$ |

A reference cantilever deflection–piezo displacement curves were obtained by measuring on an alumina substrate and a silicon wafer. As shown in Fig. 4, the deflection of the fiber ($\delta$) is the difference between the loading and the reference curve. A complete force curve contained four regions in Fig. 4; (a) the tip was far from the sample. There was no interaction and no cantilever deflection. Long- and short-range tip–sample interactions caused the cantilever to deflect (snap-in) as the stage extended and brought the sample closer to the tip, (b) when the tip contacted the surface, the stage movement and cantilever deflection became coupled, which appeared in the curve as a straight line (contact line,) (c) at this point, the direction of the sample motion was inverted and the tip was withdrawn from the sample, and (d) at a certain distance the tip was detached from the sample (snap-out) and the cantilever came back to its equilibrium position. In order to calculate $\delta$, the point of contact or height offset, $z_0$, and the deflection offset, $d_0$, for the reference and $z$ and $d$ for the sample nanofiber were determined [31].

$$\delta = (z - z_0) - (d - d_0) \tag{2}$$

The elastic modulus of nanofibers was calculated from beam bending theory given by Eq. (3), where $L$ is the suspended length, $E$ is the elastic (Young's) modulus, $I$ is the second moment area of the beam, and $\alpha = 192$ for a clamped beam ($I = \pi D^4/64$ for a filled cylinder).

$$E = \frac{F L^3}{192\,\delta\, I} \tag{3}$$

Mean Young's moduli for $TiO_2$ and $TiO_2$/PVP nanofibers were 0.9 and 75.6 GPa, respectively (Table 1). However, the $E$ values of $TiO_2$ sample is considerably low compared to bulk $TiO_2$. This difference can be explained by the following reasons: (i) the effect of the crystal orientation [32], (ii) diffusional creep at room temperature, and (iii) neglected shear deformations. With the large volume fraction of grain boundaries in nanocrystalline materials, initial publications on the deformation of nanocrystalline materials suggested the presence of diffusional creep at room temperature in pure copper and $TiO_2$ [33]. Morris et al. have also reported that the diffusional creep rate of polycrystalline materials may be enhanced by reducing the crystal size, and by increasing the boundary diffusivity [18]. As seen from Fig. 5, the scatter in $E$ values obtained from Eq. (3), might be due to the load point being off-center with respect to the beam span and the uncertainties in fiber dimensions and spring constant of the cantilever which affects the measured load. Although shear deformations were neglected in this study, the increase in fiber diameter significantly decreases $E$ values, this may be

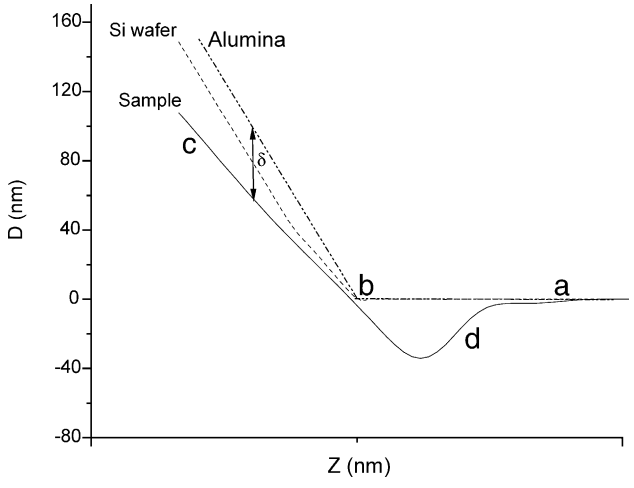


Fig. 4. Examples of cantilever deflection ($D$) vs. sample height curves ($Z$).

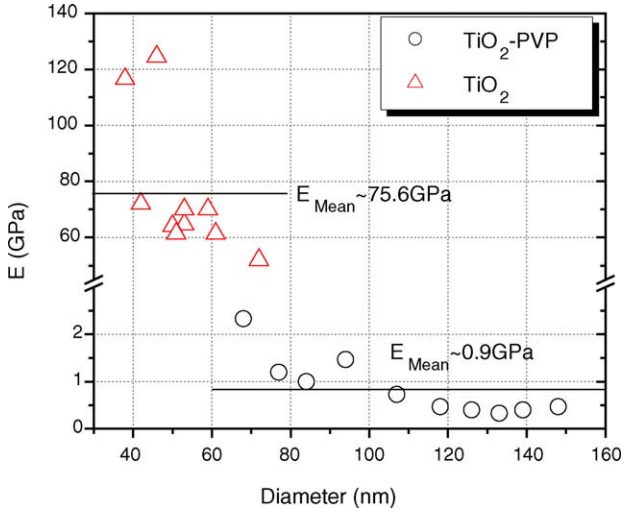


Fig. 5. Young's modulus ($E$) vs. diameter of $TiO_2$–PVP and $TiO_2$ nanofibers.

attributed to the fact that at relatively low length-to-diameter ($L/D$) ratios shear deformations become an important contribution.

## 4. Conclusion

Both PVP/$TiO_2$ and $TiO_2$ electrospun nanofibers were readily obtained by electrospinning. The elastic (Young's) moduli of the nanofibers were determined through the AFM three-point bending test. This technique successfully demonstrated the nanomechanical study of individual ceramic nanofibers and polymer–ceramic composite nanofibers.

## Acknowledgments

Authors acknowledge the National Science Foundation-Particle Engineering Research Center (NSF-PERC) at the University of Florida for financial support of this research (NSF Grant No. EEC-94-02989) and the NATO fellowship for Cagri Tekmen.

## References

[1] A. Fujishima, K. Honda, Nature 238 (1972) 37–38.
[2] P.-A. Brugger, P. Cuendet, M. Grätzel, J. Am. Chem. Soc. 103 (1981) 2923–2927.
[3] P.V. Kamat, Chem. Rev. 93 (1993) 267–300.
[4] M.A. Fox, M.T. Dulay, Chem. Rev. 93 (1993) 341–357.
[5] A. Hagfeldt, M. Grätzel, Chem. Rev. 95 (1995) 49–68.
[6] M.R. Hoffmann, S.T. Martin, W. Choi, D.W. Bahnemann, Chem. Rev. 95 (1995) 69–96.
[7] A.L. Linsebigler, G. Lu, J.T. Yates Jr., Chem. Rev. 95 (1995) 735–758.
[8] A. Mills, S.L. Hunte, J. Photochem. Photobiol. A 108 (1997) 1–35.
[9] A. Fujishima, T.N. Rao, D.A. Tryk, J. Photochem. Photobiol. C 1 (2000) 1–21.
[10] S.-H. Lee, S. Pumprueg, B. Moudgil, W. Sigmund, Colloids Surf. A 40 (2005) 93–98.
[11] D.M. Antonelli, J.Y. Ying, Angew. Chem. Int. Ed. Engl. 34 (1995) 2014–2017.
[12] P. Yang, D. Zhao, D.I. Margolese, B.F. Chmelka, G.D. Stucky, Chem. Matter 11 (1999) 2813–2826.
[13] Y. Lin, G.S. Wu, X.Y. Yuan, T. Xie, L.D. Zhang, J. Phys.: Condens. Matter 15 (2003) 2922–2971.
[14] V.V. Guliants, M.A. Carreon, Y.S. Lin, J. Membr. Sci. 235 (2004) 53–72.
[15] D. Li, Y. Xia, Nano Lett. 3 (2003) 555–560.
[16] S. Madhugiri, B. Sun, P.G. Smirniotis, J.P. Ferraris, K.J. Balkus Jr., Microporous Mesoporous Mater. 69 (2004) 77–83.
[17] S.-H. Lee, W.M. Sigmund, J. Nanosci. Nanotech. (2005) submitted for publication.
[18] J. Karch, R. Birringer, H. Gleiter, Nature 330 (1987) 556–558.
[19] J. Doshi, D.H. Reneker, J. Electrostat. 35 (1995) 151–160.
[20] D. Adams, Nature 411 (2001) 236.
[21] Z.-M. Huang, Y.-Z. Zhang, M. Kotaki, S. Ramakrishna, Compos. Sci. Technol. 63 (2003) 2223–2253.
[22] H. Dai, J. Gong, H. Kim, D. Lee, Nanotechniques 13 (2002) 674–677.
[23] P. Viswanathamurthi, N. Bhattarai, H.Y. Kim, D.R. Lee, S.R. Kim, M.A. Morris, Chem. Phys. Lett. 374 (2003) 79–84.
[24] P. Viswanathamurthi, N. Bhattarai, C.K. Kim, H.Y. Kim, D.R. Lee, Inorg. Chem. Commun. 7 (2004) 679–682.
[25] E.W. Wong, P.E. Sheehan, C.M. Liber, Science 277 (1997) 1971–1975.
[26] J.-P. Salvetat, G. Andrew, D. Briggs, R.R. Bacsa, A.J. Kulik, T. Stockli, N.A. Burnham, L. Forro, Phys. Rev. Lett. 82 (1999) 944–947.
[27] J.P. Salvetat, A.J. Kulik, J.M. Bonard, G. Andrew, D. Briggs, T. Stockli, K. Metenier, S. Bonnamy, F. Beguin, N.A. Burnham, L. Forro, Adv. Mater. 11 (1999) 161–165.
[28] E.P.S. Tan, C.T. Lim, Appl. Phys. Lett. 84 (2004) 1603–1605.
[29] Z.L. Wang, P. Poncharal, W.A. de Heer, J. Phys. Chem. Solids 61 (2000) 1025–1030.
[30] Z.L. Wang, P. Poncharal, W.A. de Heer, Pure Appl. Chem. 72 (2000) 209–219.
[31] N.P. D'Costa, J.H. Hoh, Rev. Sci. Instrum. 66 (1995) 5096–5097.
[32] K. Kurosaki, D. Setoyama, J. Matsunaga, S. Yamanaka, J. Alloys Compounds, in press.
[33] R.S. Mishra, S.X. McFadden, R.Z. Valiev, A.K. Mukherjee, JOM-US 51 (1999) 37–40.